ISSN 2278-3091
Volume 9 No.2, March -April 2020
International Journal of Advanced Trends in Computer Science and Engineering
Available Online at http://www.warse.org/IJATCSE/static/pdf/file/ijatcse20922020.pdf
https://doi.org/10.30534/ijatcse/2020/20922020

Autism Detection using r-fMRI: Subspace Approximation and CNN Based Approach

Daya Gupta[1*], Ishani Vij[2*], Mansi Gupta[3*]
[1]Delhi Technological University, India, dgupta@dce.ac.in
[2]Delhi Technological University, India, ishanivij11@gmail.com
[3]Delhi Technological University, India, mansigupta_bt2k16@dtu.ac.in

ABSTRACT

Autism spectrum disorder (ASD) is a heterogeneous disorder that causes impaired social interactions and altered behavioral patterns. It is currently diagnosed by assessing the developmental screenings, followed by a diagnostic evaluation of an individual using standard screening and diagnostic tools. However, a more concrete diagnostic method is required to get hold of the underlying cause of the disorder to ensure better treatment and prevention of the disorder. Recent research on ASD has shown resting state functional magnetic resonance imaging (r-fMRI) as a useful tool for classification of ASD and neurotypical subjects. However, due to the large dimensionality of fMRI scans, directly applying classification methods to the data results in high computational cost. In order to avoid the curse of dimensionality , we propose a combined multistage SAAK transform and CNN based approach which selects the most relevant and discriminative features without losing any information and uses them for a more accurate and less computationally expensive classification of ASD subjects from typically developing controls. A classification accuracy of 74.55% is achieved using the proposed method. We show that the performance of the proposed approach of classification using ABIDE dataset is comparable to that of standalone CNN while being less computationally intensive.

Key words : ABIDE, Autism Spectrum Disorder, Convolutional Neural Network (CNN), Karhunen- Loeve Transform (KLT), subspace approximation

1. INTRODUCTION

Autism Spectrum Disorder is a neurological and developmental disorder that affects the overall cognitive, social, emotional and physical health of an individual. It is characterised by a broad range of conditions, due to which the disease is referred to as a spectrum.

**The authors contributed equally to this work.*

These impact the nervous system and cause uneasy social interactions, difficulty in communication, restricted and repetitive behaviours and frequent sensory overloads. It is found to occur in more than 1% of the global population. Currently there is no single notion regarding the underlying causes of the disorder. Medical professionals diagnose ASD by analysing the behaviour and development of the child using a range of screening and diagnostic tools like Autism Diagnosis Interview- Revised [1], Childhood Autism Rating Scale (CARS) [2]. The reliability of these diagnostic methods remains questionable as they are prone to misdiagnosis [3]. Moreover, these methods give no information about the biological aspects of the disorder. To get a clearer idea about the underlying brain activity of autistic individuals, an inclination towards exploring the brain variance between healthy and diseased populations based on neuroimaging data has been observed.

However, given the high dimensionality of neuroimaging data, directly applying machine learning models for classification turns out to be computationally expensive. C. Jay Kuo and Yueru Chen proposed a multi-stage Subspace approximation with augmented kernels (SAAK) transform method for feature extraction. In this work, we borrow the SAAK transform method from [4] and propose a combined SAAK transform and CNN based approach for classifying the subjects as autistic and neurotypical (healthy) individuals. This approach reduces the computational cost without compromising on the accuracy of classification. We consider the functional magnetic resonance imaging (r-fMRI) scans of the subjects and the associated Blood Oxygen Level Dependent (BOLD) time series signals to build connectivity matrices, which act as input to the model. Each stage of SAAK transform reduces the dimensionality of the feature space. It also nullifies the rectification loss due to the ReLU layer by augmenting a negative kernel to all the kernels obtained. Here we point out a major difference between the ReLU layer in CNN and that in SAAK transform.

Traditionally CNNs have given state-of-the-art results in image analysis problems. Multiple convolution and pooling layers enable repeated extraction and processing of features till one gets the final features, which exhibit high robustness

and do not show changes with transformations in the input. The feature extraction step imposes constraints when dealing with a large sample size and high dimensionality data such as ABIDE dataset. SAAK transform acts as a computationally less expensive alternative for extracting relevant high level features from the data.

The rest of this paper is organised as follows: In section 2 we discuss the methods implemented so far in this field, followed by a thorough explanation of the proposed approach in Section 3. Section 4 and 5 contain the experimental details and a brief description of the experiments conducted in this study. Section 6 and 7 present the classification results, followed by a comprehensive discussion. Concluding remarks are presented in section 8.

2. LITERATURE SURVEY

Ample of studies have used neuroimaging data obtained using magnetic resonance imaging (MRI) for the classification of ASD. With the advent of MRI as a medical imaging technique, researchers have been able to gain deeper knowledge about the pathology of the disorder [5] [6] [7]. It generates detailed images of the internal organs and tissues, along with their working using strong magnetic fields and radio waves. There are two variants of MRI: structural MRI and functional MRI. Structural MRI is a technique for examining the anatomy and pathology of the brain. The studies for ASD detection conducted using structural MRI [8] [9] [10] used features like volume, surface and thickness as parameters for classification. Apart from structural alterations, autistic and normal individuals also exhibit differences in underlying brain connectivity [11] [12] [13]. The second technique of MRI, called functional MRI, is used to cap these differences. In functional MRI, the level of interaction between the different components of the brain, which may or may not be physically connected are measured. The brain activity is examined by detecting changes in the Blood Oxygen Level Dependent (BOLD) signals. It relies on the fact that cerebral blood flow and neuronal activities are coupled i.e. the blood flow to a brain region increases when that part of the brain is in use [14].

Various studies have used pairwise correlations between different regions of interest (ROIs) as features to define connectivity matrices for the subjects [13] [15] and then implemented supervised learning methods like SVM [16] and leave-one-out classifier [17], as well as CNN [18] for classification. Subbaraju et al. (2017) achieved an accuracy of 77.3% using a combined spatial filter and SVM classifier. Their method selects the most discriminative features using a spatial filter by orthogonally projecting the connectivity matrices of BOLD signals of ASD and control individuals, and feeds them to an SVM classifier. Another work by Sarah et al. (2019) used a graph based classification where they viewed the brain structure as a graph, with the ROIs as nodes and BOLD signals as edges of the graph, and used graph signal processing to obtain features related to the frequency content of the signals. A decision tree trained using these features for 452 subjects gave a classification accuracy of 73.5%. Studies that used fMRI data collected from a single site have achieved accuracy as high as 97% (Just et al., 2014). Plitt et al. (2015) compared the classifications of various machine learning algorithms on the scans of 178 ASD and IQ matched neurotypical males, and achieved a peak accuracy of 76.67% with ridge regression method. Relatively better classification is performed when sample size is small, typically constrained to around 100 participants (Arbabshirani et al., 2016), while it experiences a considerable drop when the sample size is large or in case of multi- site data. (Nielson et al., 2013).

In this study, we use data collected at multiple sites and from people of varied demographic conditions for a more robust study.

3. PROPOSED APPROACH

Here we present our strategy to adopt a combined subspace approximation with augmented kernel (SAAK) transform and CNN based approach for classification. Our data consists of 4-dimensional (time- series) fMRI scans of the subjects. Different parcellations of the brain, called regions of interest (ROI), are defined by various atlases. These atlases were used to obtain association matrices for the subjects [19]. We start by building a brain connectivity matrix for each subject. A connectivity matrix helps to quantitatively visualise the strength of functional connections. It reflects the pairwise functional connectivity between voxels of different regions of the brain and is created using the averaged Blood Oxygen Level Dependent (BOLD) time-series signals. These signals are extracted from the regions of interest defined by an atlas. The connectivity between ROIs is estimated using correlation between the time- series signals. We used three different methods for calculating the entries of the matrices: partial correlation, Pearson correlation and tangent space embedding [20]. An illustration of this approach is shown in Figure 1.

3.1 Subspace Approximation

The connectivity matrices obtained so far are of size $N \times N$, where N is the number of regions the brain is divided into, giving us N^2 features corresponding to each data item. We

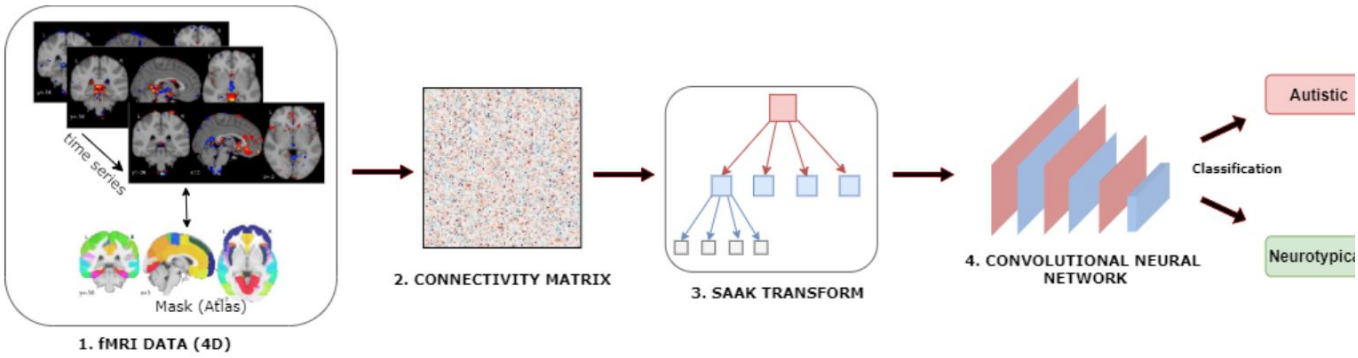

Figure 1: Illustration of the proposed approach

seek to reduce the feature space while retaining as much information as possible. This is done by transforming the data to a linear subspace with an orthogonal basis using KLT in multiple stages.

First the connectivity matrices are scaled to have dimensions that are the n^{th} power of 2, for some $n \in I^+$. These scaled connectivity matrices act as the input to the multistage SAAK transform. We then obtain the KLT basis functions, b_k , for the input vectors $f \in R_n$. The requirement for multiple stages arises as it is practically infeasible to conduct KLT on the entire input matrix due to its large size , as explained below.

3.2 Multiple Stages

For the determination of the KL transform of a feature set, it is first required to calculate the covariance matrix. Let $X=[x_1\, x_2 \ldots x_N]^T$ denote the initial feature matrix of a subject. The covariance matrix of *X* is computed as:

$$C_X = \frac{1}{N}\sum_{i=1}^{N}(x_i x_i^{'}) \tag{1}$$

Now, the eigenvectors, *V*, of the covariance matrix are arranged into rows to form the orthogonal transformation matrix, *T*.

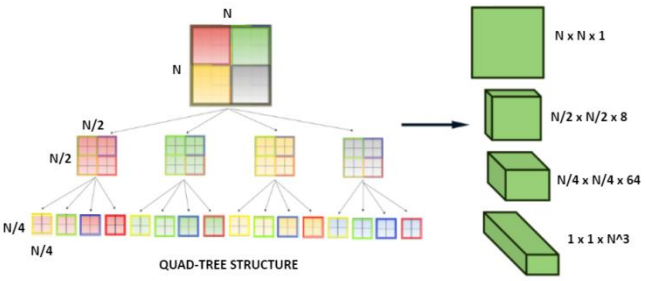

Figure 2: Multistage SAAK Transform quad-tree structure

Thus, the transformation matrices in KLT are dependent on the feature set, more precisely on its covariance matrix. For a feature set with dimension $N \times N$, the matrix will be of the order N^4. In case of large values of *N*, the transformation will require non- trivial computations, suggesting the infeasibility of application. Consequently, large sized connectivity matrices are transformed into a smaller subspace by recursively decomposing them into smaller parts. The application of KLT at each level brings down the dimensions of the feature set by a factor of two.

Hence, we decompose the matrices into four smaller non-overlapping parts in each stage, eventually forming a quad-tree structure. Each node of this tree is half the size of its parent node, the leaf nodes being of the size 2×2. KLT is applied at each level of the tree to obtain the basis functions.. All the stages of SAAK transform are cascaded in a bottom up manner. A sign-confusion problem occurs due to the recursive application of KLT [18]. Therefore, a ReLU activation function is introduced between two successive transforms. Figure 2 shows the formation of quad tree structure in multistage saak transform, useful for transforming images with dimensions $(N \times N \times 1)$ into dimensions $(1 \times M \times M)$, where M denotes N^3.

3.3 Kernel Augmentation

The addition of the ReLU operation between the KLT transforms is accompanied by an increased rectification loss. We attempt to bring down the rectification loss by using kernel augmentation [4]. We generate $(N-1)$ pairs of AC kernels, in addition to a DC kernel, using the KLT basis functions obtained above. We retain the projections on the DC kernels and pass the AC projections through the ReLU activation function. The DC vector is represented as

$$a_0 = \frac{1}{N}(1, 1, \ldots, 1)^T \tag{2}$$

Each AC kernel pair consists of a positive kernel, a_{2k-1}, augmented with its negative vector, a_{2k}. These are generated using the basis functions, b_k, according to as:

$$a_{2k-1} = b_k, \quad a_{2k} = -b_k, \quad k = 1, 2, \ldots, N-1 \tag{3}$$

The input vectors, *f*, are projected onto these kernels to yield a projection vector

$$p = (p_0, p_1, \ldots, p_{(2N-1)})^T \quad \in R^{2N-1} \tag{4}$$

where $p_k = a_k^T f$ represents the projection of *f* on kernel a_k. The above process representing a single stage SAAK transform is repeated till signed KLT coefficients of dimensions $1 \times 1 \times 2^{3t}$ are obtained, where $2^t \times 2^t$ is the initial size of the connectivity matrix. All the projection vectors except the DC projection p_0 are passed through the ReLU function and we obtain the SAAK coefficients, *o,* as:

$$o = (o_0, o_1, \ldots, o_{(2N-1)})^T \quad \in R^{2N-1} \tag{5}$$

where, $o_0 = p_0$ (DC projection retained) and for *k = 1, ..., N*:

$$o_{2k-1} = p_{2k-1} \quad and \quad o_{2k} = 0 \quad , if \ p_{2k-1} > 0 \tag{6}$$

$$o_{2k-1} = 0 \quad and \quad o_{2k} = p_{2k} \quad , if \ p_{2k} > 0 \tag{7}$$

Unlike CNN where the activation of input signals introduces non- linearity in the output, we preserve all the convolution input by augmenting the kernels with their negatives. This way, there will be a positive/negative correlation pair of each input vector with kernel pair (a_{2k-1}, a_{2k}). ReLU will allow one correlation from the pair to pass through it and will block the other one.

3.4 Feature Selection

Finally, we calculate and compare the F- score of the coefficients to select the most important features. The discriminative power of a feature is directly proportional to its F-test score, hence features with highest F-test scores are chosen to form the final feature vectors. F- score is computed as:

$$F = \frac{larger\ sample\ variance}{smaller\ sample\ variance} \tag{8}$$

The larger sample variance (LSV) and smaller sample variance (SSV) can be written respectively as:

$$LSV = \frac{\sum_{i=1}^{K} n_i (\bar{X}_i - \bar{X})^2}{(K-1)} \tag{9}$$

where, $\bar{X}$ is the mean of the entire data, $\bar{X}_i$ is the mean of the i^{th} classification group, n_i represents the number of observations in the i^{th} group, and *K* is the total number of groups.

$$SSV = \frac{\sum_{i=1}^{K} \sum_{j=1}^{n_i} (X_{ij} - \bar{X}_i)^2}{(N-K)} \tag{10}$$

where, X_{ij} is the j^{th}observation in the i^{th}group and *N* is the total size of the sample.

In this study, for the CC200 atlas, the initial size of the connectivity matrix is 200 x 200. The number of features was reduced to 7294 after the multistage SAAK transform. After calculating the F-score for all the features, we chose 1000 top features with the highest F- scores.

3.5 CNN

Our CNN architecture, represented in Figure 3, consists of three convolution layers interspersed with pooling layers followed by a fully connected layer which computes disease probability and is subsequently used for classification. The model has a batch size of 32 and was trained for 20 epochs. To avoid overfitting the data, the learning rate of CNN was set to 0.001 and momentum to 0.9.

Note that Figure 3 is only for architectural representational purposes. The actual CNN used is one dimensional in nature and takes as input the output of SAAK transform.

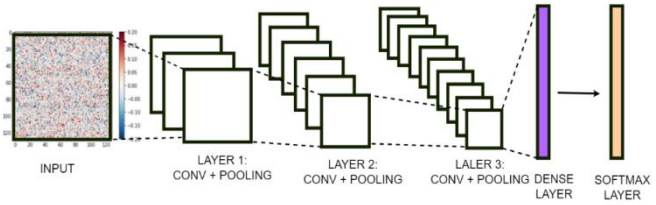

Figure 3: Convolutional neural network architecture

4. MATERIALS AND METHODS

4.1 Data and participants

The data used for this study was downloaded from the Autism Brain Imaging Data Exchange (ABIDE) project (http://fcon_1000.projects.nitrc.org/indi/abide/). The data comprises of rs-fMRI scans of subjects, along with phenotypic information such as subject identity number, age, sex, assessment scores (IQ test, social interaction, communication etc.) for each subject.

Due to the difference in conditions (eye status during scan i.e. opened/ closed, taken stimulants 24 hours prior to scan, etc) while sampling the data, and the variety in demographic conditions of the subjects (age, sex, handedness, etc) the dataset shows a significant extent of heterogeneity. Hence, making use of the phenotypic information available to us, we define the participants of this study as the subjects who met all the following criteria:

- Eye status during rest scan- open
- Quality control (manual assessment)

Table 1 shows the demographic details of the 609 participants.

Table 1: Participant classification

Gender	Individual Orientation

	ASD	***Neurotypival***
Male	252	252
Female	36	69
Age (<=20)	242	270
Age (>20)	46	51

4.2 Preprocessing

The ABIDE consortium shared a preprocessed version of the data as a part of the Preprocessed Connectomes Project (PCP). Out of the four available pipelines, we chose the data which was pre-processed according to the C-PAC (Configurable Pipeline for the Analysis of Connectomes) pipeline. The data obtained was corrected by reslicing for head-motion, intensity normalisation (with global mean = 1000), motion realignment, and nuisance signal removal (due to physiological processes like heartbeat and respiration). The data were transformed from the individual native space to the Montreal Neurological Institute (MNI) space. Global signal regression, however, is not used in this study. Steps involved in data processing are shown in Figure 4.

Figure 4: Data preprocessing workflow

5. EXPERIMENTS

The following experiments were carried out in this study:

1. Classification Model: Experiments were conducted to determine the best classifier for classification of data before applying SAAK transform as well as that for linear SAAK transform output. SAAK transform output was classified using linear support vector classifier (SVC), Dense Net and CNN.
2. Atlas for time-series extraction: Atlas for time-series extraction: Out of the seven atlases used by PCP for ROI time-series extraction, we consider the following five atlases for the input data and compare the classification performances: Harvard-Oxford (HO), Craddock 200 (CC200), Eickhoff-Zilles (EZ), Talaraich and Tournoux (TT) and Dosenbach 160 (DOZ160).
3. Type of connectivity matrix: Connectivity matrix for a subject is estimated based on its time-series data. Three kinds of connectivity measures: partial correlation, correlation and tangent space embedding were used to construct the connectivity matrix and the classification ability of the model corresponding to each of these was analysed .
4. Time demand of CNN vs proposed approach: Computational efficiency of CNN and proposed combined SAAK and CNN approach was evaluated and compared.

6. RESULTS

6.1 Performance comparison of proposed approach and other approaches

Performance of the proposed approach was compared with various machine learning and deep learning classification models present in the literature. Table 2 shows the cross-validation accuracy for all the atlases used in the PCP for ROI time series extraction. These scores are corresponding to the partial correlation connectivity matrices. Five classification approaches viz. Decision tree, SVC, dense net, CNN and SAAK + CNN were evaluated. CNN achieved classification accuracy of 75.23 percent, marginally higher than accuracy of 74.55 percent obtained using the proposed approach.

Table 2: Performance of classifiers with different atlases

Brain Atlas	**Classifier Accuracy (%)**				
	Decision Tree	***SVC***	***Dense Net***	***CNN***	***SAAK + CNN***
HO	62.12	64.35	67.71	71.92	71.26
CC200	64.55	65.78	69.20	75.23	**74.55**
EZ	64.98	65.21	64.88	72.67	71.98
TT	60.23	60.47	62.55	69.04	68.39
DOZ160	62.63	59.71	68.23	70.95	70.31

Table 3: Performance of different correlation measures

Correlation Measure	**Classifier Accuracy (%)**		
	SAAK+SVC	***SAAK + Dense Net***	***SAAK+CNN***
Partial	68.84	71.62	**74.55**
Pearson	66.29	69.13	70.61
Tangent	68.51	70.02	74.46

Table 3 presents classification accuracy corresponding to the different correlation measures used for constructing the correlation matrix, using the CC200 atlas.

6.2. Computational Efficiency

All experiments were conducted in python. on a system with windows 10 operating system, core i7 processor and 8 GB RAM. Execution time of both CNN and proposed approach are as follows:

- CNN : 7 minutes 23 sec
- SAAK + CNN : 3 min 9 sec

6.3 Filtering of Signals

Band pass filtered and non band pass filtered signals were evaluated and the observed accuracy of signals after band pass filtering was found to be marginally better.

- Band pass filtering (0.01 - 0.073 Hz): 74.55% accuracy
- Non band pass filtered : 74.39% accuracy

7. DISCUSSIONS

We carried out a detailed experimental evaluation of our proposed approach on the ABIDE dataset and observed that classification using the proposed method gave results comparable to other state-of-the-art methods for large data sets while being more computationally effective.

7.1 Impact of connectivity parameterisation

We computed the connectivity matrices of subjects to use them as input to the model. The connectivity matrices were established using three techniques - Pearson correlation, partial correlation and tangent space embedding (which is a combination of both), and the performance of the model in each case was studied. The best accuracy was obtained using a partial correlation based network. Only a marginal difference in accuracy was seen between the partial correlation and tangent space methods. The tangent space method has a strong mathematical foundation and is being explored in various studies. This result can be backed up by the findings of previous studies on correlation methods which suggest the Pearson method only reflects the marginal association between network nodes and does not capture the true or direct functional connection between them. For example, a large correlation between a pair of nodes can appear due to their common connections to a third-party node, even if the two nodes are not directly connected. [21], [22]. Figure 5 shows the connectivity matrices for the three types of connectivity measures: pearson, partial and tangent.

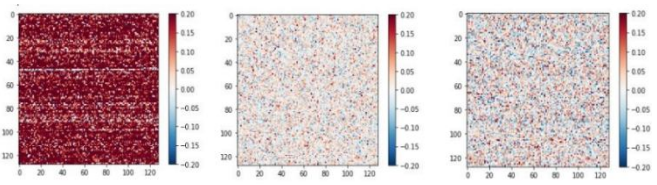

Figure 5: Pearson, partial and tangent correlation matrices

7.2. Impact of parcellation scheme on prediction accuracy

BOLD signals inside the brain are averaged at parcel level. Therefore, both coordinates of the brain regions defined and the size of regions have an effect on the signal content. Hence, we analyse the impact of parcellation scheme on the accuracy of prediction by considering five atlases.
We evaluated the atlases against the proposed method as well as some other state-of-the-art methods on the same dataset. We found out that the SAAK transform classification gave better results than all other methods tested. Further, ROIs defined using the functional CC200 atlas outperformed all other atlases shown in the table. This shows that classification performance is indeed influenced by the atlas selected.

7.3 Impact of frequency of signals

The extracted time- series signals were band-pass filtered to obtain signals in the frequency band 0.01Hz - 0.073Hz (Slow 4 and Slow 5 bands). We implemented our approach with both filtered and non- filtered signals. The filtered signals gave a slightly better discrimination performance over the non- filtered ones. However, we could not establish a clear preference between the two.

7.4 Computational efficiency: SAAK vs CNN

Convolutional neural networks (CNN) and SAAK transform both employ the ReLU activation function. However, there is a fundamental difference in the way these techniques determine their filter weights. In CNN, a supervised learning approach is used to determine the weights. The mapping between input and their corresponding output labels is used to update the weights iteratively. Usually, back-propagation of the loss helps update weights, thereby reducing the classification error. On the other hand, multi-stage SAAK transform uses the second-order statistics of the input vector to select the filter weights. While CNNs usually require a large number of iterations, both input vector, and associated labels to learn the weights, SAAK transform is a feed-forward single-pass process. Using just the input vector, SAAK transform effectively deduces the filter weights in a single pass. This makes SAAK transform a simple and a faster alternative to CNN.

8. CONCLUSION

As of present, no scientific method is used in industry for diagnosis and subsequent management of ASD. Recent years have shown a rise in ASD research [23], [24] but this has been limited by the high dimensionality of images. In this paper, we proposed a SAAK transform based classifier to identify ASD affected individuals from healthy individuals. We analysed the functional connectomes using different atlases, and selected the best parcellation scheme. We also showed that our proposed approach achieved classification accuracy comparable to the existing machine- learning state of the art approach, while being significantly more efficient computationally.

REFERENCES

1. O. Tadevosyan-Leyfer, M. Dowd, R. Mankoski, B. Winklosky, S. Putnam, L. McGrath, H. Tager-Flusberg, and S. E. Folstein, "**A principal components analysis of the autism diagnostic interview-revised**," Journal of

the American Academy of Child & Adolescent Psychiatry, vol. 42, no. 7, pp. 864–872, 2003.
2. M. E. Van Bourgondien, L. M. Marcus, and E. Schopler, "**Comparison of dsm-iii-r and childhood autism rating scale diagnoses of autism**," Journal of Autism and Developmental Disorders, vol. 22, no. 4, pp. 493–506, 1992. https://doi.org/10.1007/BF01046324
3. T. Charman and K. Gotham, "**Measurement issues: Screening and diagnostic instruments for autism spectrum disorders–lessons from research and practise**," Child and adolescent mental health, vol. 18, no. 1, pp. 52– 63, 2013.
4. C.-C. J. Kuo and Y. Chen, "**On data-driven saak transform**," Journal of Visual Communication and Image Representation, vol. 50, pp. 237–246, 2018. https://doi.org/10.1016/j.jvcir.2017.11.023
5. B. Biswal, F. Zerrin Yetkin, V. M. Haughton, and J. S. Hyde, "**Functional connectivity in the motor cortex of resting human brain using echoplanar mri**," Magnetic resonance in medicine, vol. 34, no. 4, pp. 537– 541, 1995. https://doi.org/10.1002/mrm.1910340409
6. T. P. Gabrielsen, J. S. Anderson, K. G. Stephenson, J. Beck, J. B. King, R. Kellems, D. N. Top, N. C. Russell, E. Anderberg, R. A. Lundwall, et al., "**Functional mri connectivity of children with autism and low verbal and cognitive performance**," Molecular autism, vol. 9, no. 1, p. 67, 2018. https://doi.org/10.1186/s13229-018-0248-y
7. D. P. Kennedy, E. Redcay, and E. Courchesne, "**Failing to deactivate: resting functional abnormalities in autism**," Proceedings of the National Academy of Sciences, vol. 103, no. 21, pp. 8275–8280, 2006.
8. Y. Jiao, R. Chen, X. Ke, K. Chu, Z. Lu, and E. H. Herskovits, "**Predictive models of autism spectrum disorder based on brain regional cortical thickness**," Neuroimage, vol. 50, no. 2, pp. 589–599, 2010. https://doi.org/10.1016/j.neuroimage.2009.12.047
9. R.Abitha and Dr S. Mary Vennila, " **CBARG-Cultural Based Optimized Association Rule Generation Method to Improve Knowledge Discovery in Autism Spectrum Disorder**," International Journal of Advanced Trends in Computer Science and Engineering, vol. 8, no. 6, pp. 3327-22 https://doi.org/10.30534/ijatcse/2019/104862019
10. C. Ecker, V. Rocha-Rego, P. Johnston, J. Mourao-Miranda, A. Marquand, E. M. Daly, M. J. Brammer, C. Murphy, D. G. Murphy, M. A. Consortium, et al., "**Investigating the predictive value of whole-brain structural mr scans in autism: a pattern classification approach**," Neuroimage, vol. 49, no. 1, pp. 44–56, 2010.
11. D. P. Kennedy and E. Courchesne, "**The intrinsic functional organization of the brain is altered in autism**," Neuroimage, vol. 39, no. 4, pp. 1877– 1885, 2008. https://doi.org/10.1016/j.neuroimage.2007.10.052
12. V. L. Cherkassky, R. K. Kana, T. A. Keller, and M. A. Just, "**Functional connectivity in a baseline resting-state network in autism**," Neuroreport, vol. 17, no. 16, pp. 1687–1690, 2006.
13. C. Ecker, A. Marquand, J. Mourao-Miranda, P. Johnston, E. M. Daly, ˜ M. J. Brammer, S. Maltezos, C. M. Murphy, D. Robertson, S. C. Williams, et al., "**Describing the brain in autism in five dimensions—magnetic resonance imaging-assisted diagnosis of autism spectrum disorder using a multiparameter classification approach**," Journal of Neuroscience, vol. 30, no. 32, pp. 10612–10623, 2010.
14. O. B. Paulson, S. G. Hasselbalch, E. Rostrup, G. M. Knudsen, and D. Pelligrino, "**Cerebral blood flow response to functional activation**," Journal of Cerebral Blood Flow & Metabolism, vol. 30, no. 1, pp. 2–14, 2010. https://doi.org/10.1038/jcbfm.2009.188
15. F. Zhao, H. Zhang, I. Rekik, Z. An, and D. Shen, "**Diagnosis of autism spectrum disorders using multi-level high-order functional networks derived from resting-state functional mri**," Frontiers in human neuroscience, vol. 12, p. 184, 2018.
16. H. Chen, X. Duan, F. Liu, F. Lu, X. Ma, Y. Zhang, L. Q. Uddin, and H. Chen, "**Multivariate classification of autism spectrum disorder using frequency-specific resting-state functional connectivity—a multicenter study**," Progress in Neuro-Psychopharmacology and Biological Psychiatry, vol. 64, pp. 1–9, 2016. https://doi.org/10.1016/j.pnpbp.2015.06.014
17. J. A. Nielsen, B. A. Zielinski, P. T. Fletcher, A. L. Alexander, N. Lange, E. D. Bigler, J. E. Lainhart, and J. S. Anderson, "**Multisite functional connectivity mri classification of autism: Abide results**," Frontiers in human neuroscience, vol. 7, p. 599, 2013. https://doi.org/10.3389/fnhum.2013.00599
18. C.-C. J. Kuo, "**The CNN as a guided multilayer recos transform [lecture notes]**," IEEE signal processing magazine, vol. 34, no. 3, pp. 81–89, 2017. https://doi.org/10.1109/MSP.2017.2671158
19. C. Craddock, Y. Benhajali, C. Chu, F. Chouinard, A. Evans, A. Jakab, B. S. Khundrakpam, J. D. Lewis, Q. Li, M. Milham, et al., "**The neuro bureau preprocessing initiative: open sharing of preprocessed neuroimaging data and derivatives**," Neuroinformatics, vol. 41, 2013.
20. G. Varoquaux, F. Baronnet, A. Kleinschmidt, P. Fillard, and B. Thirion, "**Detection of brain functional-connectivity difference in post-stroke patients using group-level covariance modeling**," in International Conference on Medical Image Computing and Computer-Assisted Intervention, pp. 200–208, Springer, 2010. https://doi.org/10.1007/978-3-642-15705-9_25
21. S. M. Smith, K. L. Miller, G. Salimi-Khorshidi, M. Webster, C. F. Beckmann, T. E. Nichols, J. D. Ramsey,

and M. W. Woolrich, "**Network modelling methods for fmri,**" Neuroimage, vol. 54, no. 2, pp. 875–891, 2011.

22. Y. Wang, J. Kang, P. B. Kemmer, and Y. Guo, "**An efficient and reliable statistical method for estimating functional connectivity in large scale brain networks using partial correlation**," Frontiers in neuroscience, vol. 10, pp. 123, 2016. https://doi.org/10.3389/fnins.2016.00123
23. Norshuhani Zamin, Norita Md. Norwawi, Noreen Izza Arshad and Mohamad Amirul Asraf Ismail, "**Jawi Alphabot: A Jawi Teaching Robot for Children with Autism**," International Journal of Advanced Trends in Computer Science and Engineering, vol. 8, no. 1.4, pp. 363-367, 2019 https://doi.org/10.30534/ijatcse/2019/5581.42019
24. Mohamed A. Saleh, N. Marbukhari and Habibah Hashim, "**A Deep Learning Approach in Robot-Assisted Behavioral Therapy for Autistic Children**", International Journal of Advanced Trends in Computer Science and Engineering, vol. 8, no. 1.6, pp. 437-443, 2019 https://doi.org/10.30534/ijatcse/2019/6381.62019